AIAA JOURNAL
Vol. 39, No. 1, January 2001

Analytical and Computational Study of Wall Temperature Jumps in Supersonic Flow

George R. Inger*
Iowa State University, Ames, Iowa 50011
and
Peter A. Gnoffo†
NASA Langley Research Center, Hampton, Virginia 23681-0001

The local viscous–inviscid interaction field generated by a wall temperature jump on a flat plate in supersonic flow is studied in detail by the use of both a Navier–Stokes numerical code and an analytical triple-deck model. Treatment of the rapid heat transfer changes both upstream and downstream of the jump is included. Closed-form relationships for the pressure and heating variations, including upstream influence, are derived from the triple-deck theory and are found to be in good agreement with the numerical solution of the compressible Navier–Stokes equations. Such relationships not only clarify the interactive physics involved, but also are useful in preliminary design of thermal protection systems and as an insertable module to improve computational fluid dynamics code efficiency when applied to such small-scale interaction problems. Further examined is the connection between the triple-deck solution and the classical boundary-layer theory treatment of the wall temperature jump problem; the latter is shown to be similar to the far wake limit of the inner interactive behavior astride the jump.

Nomenclature

C	=	Chapman–Rubesin parameter, $\mu T_\infty / \mu_\infty T$
C_p	=	specific heat
$C_{1,2,3,4,5,6}$	=	constants in analytical solutions; Eqs. (25–28)
H	=	total enthalpy, $C_p T + u^2/2$
$\mathcal{H}$	=	enthalpy perturbation variable; Eq. (19)
J	=	0 for $X < X_J$, 1 for $X > X_J$
K_H	=	$(\gamma + 1)\lambda^{1/2} M_\infty^2 C_{\text{REF}}^{1/4} \varepsilon^2 / 4\beta^{1/2}$
L	=	reference length (see Fig. 1), equal to X_J
M	=	Mach number
$\mathcal{P}$	=	pressure perturbation variable; Eq. (20)
Pr	=	Prandtl number
p	=	static pressure
q_w	=	wall heat transfer rate
$\hat{q}$	=	q_w / q_{w0}; Eq. (26)
Re_L	=	Reynolds number $\equiv \varepsilon^{-8}$, $\rho_\infty U_\infty L / \mu_\infty$
s_e	=	v_e / U_∞, total streamline slope along the boundary-layer edge
T	=	absolute static temperature
T_t	=	freestream total temperature, $H_{0\infty} / C_p$
$\mathcal{U}$	=	streamwise velocity perturbation variable; Eq. (17)
U_∞	=	freestream velocity at edge of incoming boundary layer
u, v	=	velocity components in the x and y directions, respectively
V	=	transformed normal velocity; Sec. III.A
$\mathcal{V}$	=	normal velocity perturbation variable; Eq. (18)
X_J	=	temperature jump station
x, y	=	streamwise and normal coordinates, respectively
Y	=	transformed y coordinate; Sec. III.A
β	=	$(M_\infty^2 - 1)^{1/2}$
$\Gamma(N)$	=	gamma function of argument N
γ	=	specific heat ratio
ΔT_w	=	wall temperature jump, $T_w^+ - T_{\bar{w}}$
δ	=	boundary-layer thickness
θ	=	discontinuous jump function; Eq. (16)
κ	=	upstream influence parameter; Eqs. (25) and (26)
λ	=	Blasius solution constant, 0.332
μ	=	coefficient of viscosity $\equiv \rho\nu$
ρ	=	density
$\bar{\chi}$	=	viscous interaction parameter, $C_{\text{REF}} M_\infty^3 Re_L^{-1/2}$
ω	=	viscosity temperature-dependence exponent ($\mu \sim T^\omega$)

Subscripts

AD	=	adiabatic wall conditions
B	=	body surface
e	=	local inviscid flow conditions at boundary-layer edge
REF	=	based on reference temperature
w	=	wall surface conditions
0	=	undisturbed boundary layer ahead of interaction zone
∞	=	freestream conditions
$+, -$	=	conditions downstream and upstream of jump, respectively

Superscripts

$\hat{H}$	=	enthalpy function; Eq. (16)
$\hat{}$	=	nondimensional variables from triple-deck theory; Eqs. (1–6)

Presented as Paper 99-0226 at the 38th Aerospace Sciences Meeting, Reno, NV, 11–14 January 1999; received 10 March 1999; revision received 14 April 2000; accepted for publication 25 May 2000.

*Professor of Aerospace Engineering, Aerospace and Engineering Mechanics Department. Associate Fellow AIAA.

†Aerothermodynamics Branch, Aero/Gas Dynamics Division. Associate Fellow AIAA.

I. Introduction

THE compressible laminar viscous flow along a nonadiabatic surface that contains a temperature jump is a basic problem that arises in contemporary aerothermodynamics owing to the presence of wall material or emissivity discontinuities. It is an important problem to solve in detail because the resulting local viscous–inviscid interaction field in the vicinity of the jump contains large heat transfer surges that are of concern in thermal protection system design; it also contains many features in common with the analogous problem of flow past a jump in surface catalycity.[1] The problem is a challenging one because of the very short streamwise scale and complicated flow physics therein, which are difficult and costly to resolve even by the best of available Navier–Stokes computational fluid dynamics (CFD) codes. The present investigation addresses this wall temperature jump problem for the case of supersonic ideal

gas flow using a combined analytical–numerical approach involving a triple-deck theory analysis and a specially modified version of the well-known LAURA code.[2] Our goal is to illuminate the basic interactive physics of such temperature jumps, while providing an engineering tool for calculating important features (such as the local heat transfer behavior and upstream influence) that can be imbedded within a larger-scale CFD code.

II. Problem Definition

As schematically illustrated in Fig. 1, we consider an incoming nonadiabatic laminar boundary layer with supersonic external flow that encounters an arbitrary wall temperature jump (from T_w^- to T_w^+) at some arbitrary streamwise station L. The incoming boundary-layer profile is modeled by self-similar compressible flat plate velocity and total enthalpy profiles, and the overlaying disturbed external inviscid flow is assumed to be governed by linearized supersonic theory. Furthermore, the Reynolds number Re_L is taken to be very large such that the small parameter $\varepsilon = Re_L^{-1/8}$ is small compared to unity along with the boundary-layer thickness ratio $\delta_0/L \sim \varepsilon^4$. Finally (as well-supported by our numerical results in which CFD solutions with and without streamwise diffusion essentially overlap on the scale of Fig. 2), the effects of streamwise diffusion may be neglected even within the very short scale of the jump-generated interaction zone as long as the gas flow behaves as a continuum.

Test conditions for the flat plate are presented in Table 1. The plate is 30 cm long with a sharp leading-edge radius of 0.1 mm. The flow is laminar, steady, and two-dimensional. The Mach 6 test case is chosen to be compatible with operating conditions in the NASA Langley Research Center (LaRC) 20-in. Mach 6 facility for possible future testing. The Mach 4 and Mach 2 test conditions with $Re_L = 2.7 \times 10^6$ match the total enthalpy of the Mach 6 test condition. The sensitivity of the results to Reynolds number was checked by introducing a variation in freestream density at Mach 2 and Mach 4. The high Reynolds number, Mach 2 case most closely matches the conditions assumed in the triple-deck analysis.

The wall temperature T_w^- is set to 300 K. Three jumps in surface temperature across X_J, corresponding to $\Delta T_w/T_w^- = -0.1$, 0.1, and 0.2 are considered. Two values for $X_J = 5.06$ and 20.455 cm were simulated in the Mach 6 case to quantify the influence of leading-edge effects and boundary-layer growth; the pressure and heating relaxation phenomena being investigated here associated with the temperature jump occur on a comparable scale to these background influences. Only the results for the jump at $X_J = 20.455$ cm are presented here, and Reynolds number Re_L values presented in Table 1 are based on this location. This station is so far downstream of the nose (2046 nose radii) that the local inviscid flow pressure gradients due to nose bluntness and global displacement thickness growth are both extremely small, the local boundary-layer profile shape being that of a flat plate flow at $X = X_J$ (see Figs. 3 and 4). Comparisons of numerical simulation and triple deck theory at $X_J = 5.06$ cm are qualitatively and quantitatively similar to the comparisons that follow at $X_J = 20.455$ cm.

For purposes of preliminary orientation, Fig. 2 presents some wall pressure and local heat transfer results from the CFD code to

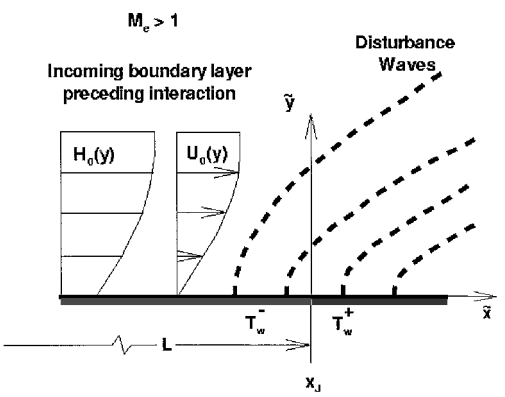

Fig. 1 Schematic of interaction generated by a wall temperature jump.

Table 1 Flat plate test conditions

M_∞	Re_L	ρ_∞, kg/m^3	V_∞, m/s	T_∞, K	T_w, K
2	2.7×10^6	3.433×10^{-1}	654.6	265.9	300
2	2.7×10^5	3.433×10^{-2}	654.6	265.9	300
4	2.7×10^6	1.263×10^{-1}	881.6	120.4	300
4	2.7×10^5	1.263×10^{-2}	881.6	120.4	300
6	2.7×10^6	5.850×10^{-2}	956.0	63.0	300

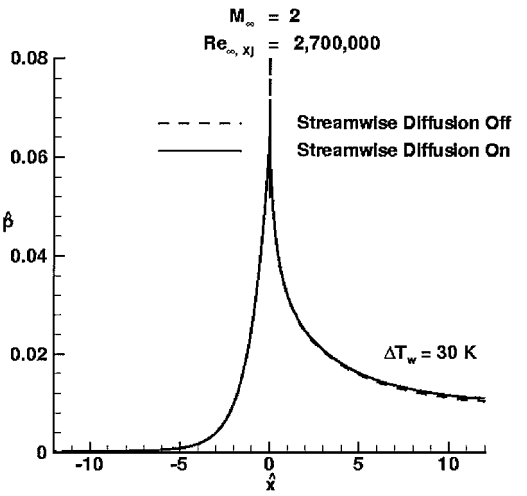

Pressure

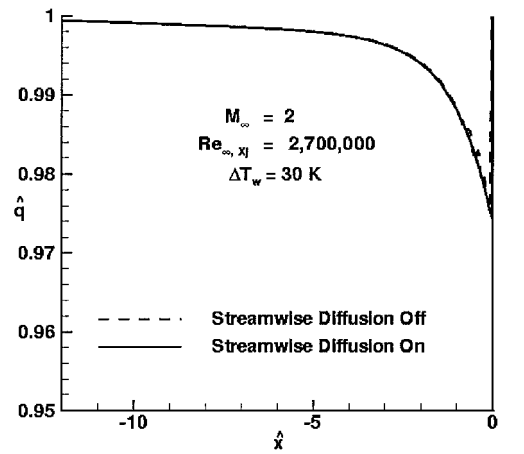

Heat transfer upstream of jump

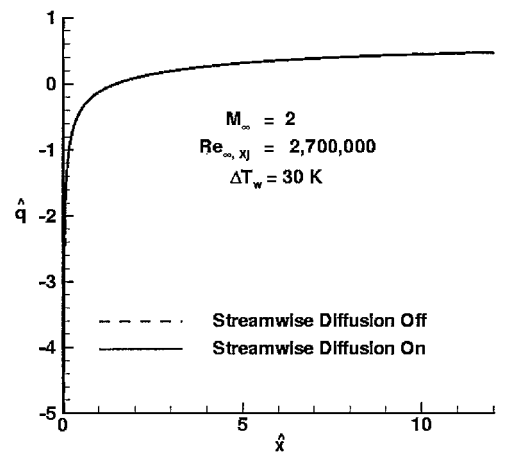

Heat transfer downstream of jump

Fig. 2 Typical interactive pressure and heating distributions for a weak T_w increase (CFD).

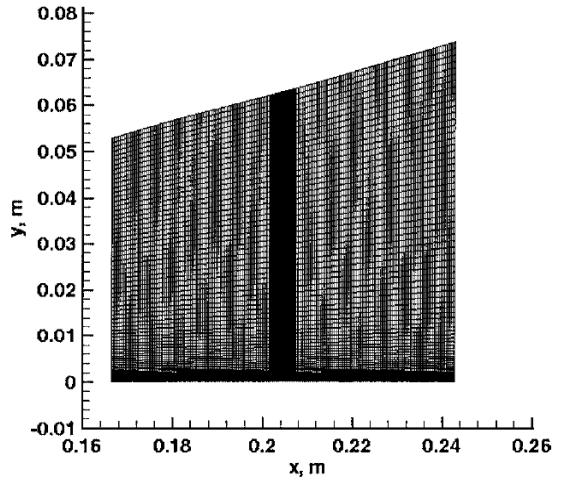

Grid

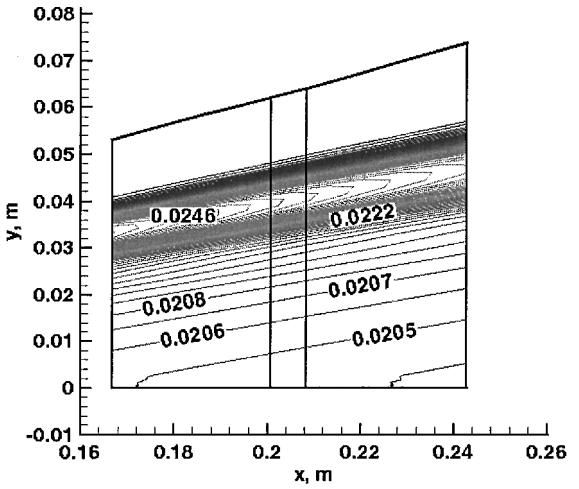

Pressure contours

Fig. 3 Test case simulation with factor 100 increase (0.03 mm) in streamwise resolution.

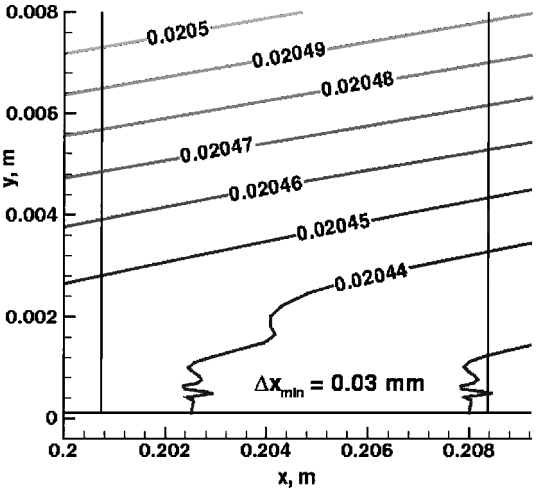

Without temperature jump

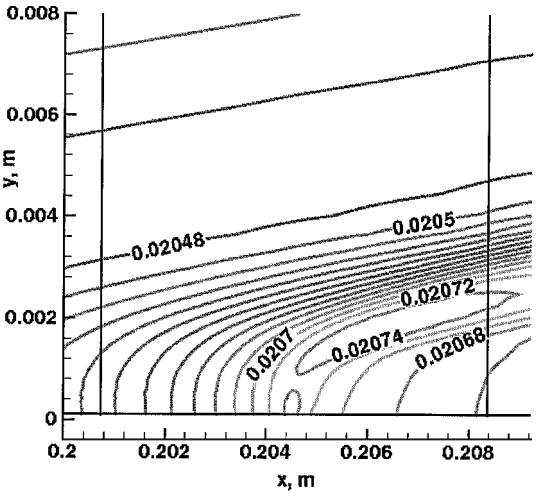

With temperature jump

Fig. 4 Comparison of pressure contours around $x_J = 20.455$ cm in embedded block with and without temperature jump.

illustrate the typical nature of the interaction zone generated by a weak (10%) wall temperature increase at Mach 2. It is seen that this small wall temperature increase generates a dispersed weak compressive disturbance with an upstream influence and a slow decay in the downstream wake region, accompanied by a drop in the local heat transfer upstream followed by rapid streamwise changes in heating around the maximum pressure rise before decaying to the new downstream wall temperature value. The influence of streamwise diffusion indicated in Fig. 2 is seen to be altogether negligible from an engineering standpoint. Clearly, understanding and analyzing such small-scale, rapid-changing thermophysics will require some powerful analytical tools: A triple-deck approach meets this need.

III. Analytical Study

A. Triple-Deck Formulation

For large Reynolds numbers, it is known that the local perturbation field caused by an abrupt disturbance in boundary conditions organizes itself into the three-layered structure[3] shown in Fig. 5. We have applied the leading asymptotic approximation $\varepsilon \rightarrow 0$ of such a triple-deck theory to treat the specific case of a wall temperature jump, where the disturbance field evidently derives from the resulting density changes (compressibility effect) in the inner deck. The analysis is formulated according to the following steps. First, the Howarth–Dorodnitzn transformation is applied into the inner deck analysis to capture the essential compressibility effect from the wall temperature jump: We thus introduce $V(X, Y) \equiv (\rho v/\rho_{ow}) + U\partial Y/\partial x$ and $\mathrm{d}Y \equiv (\rho/\rho_{ow})\,\mathrm{d}y$ along with $U(X, Y) = u(x, y)$ and $X = x$. Second, the reference temperature concept[4] is used to describe the incoming undisturbed boundary-layer profiles, and the energy equation is formulated in total enthalpy

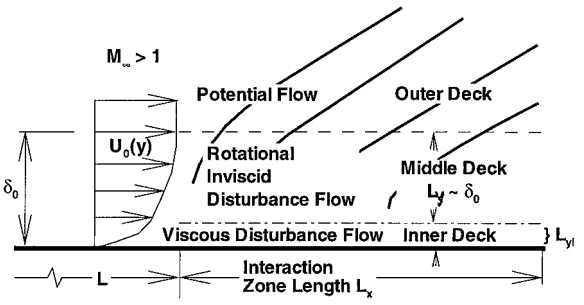

Laminar Flow: $\varepsilon = \mathrm{Re}_L^{-1/8}$, $\delta \sim \varepsilon^4 L$, $L_{yi} \sim \delta / \mathrm{Re}_L^{1/8}$, $L_x \sim \delta\ \mathrm{Re}_L^{1/8}$

Fig. 5 Triple-deck structure of the interaction zone for very large Reynolds numbers.

form to better capture the heat transfer aspects at the higher supersonic Mach numbers. Third, appropriately rescaled flow and coordinate variables are introduced, in which the governing continuity, momentum, and energy equations are expressed in nondimensional form. For $\mu \sim T^{\omega}$, these are

$$\hat{X} \equiv (X/L)\lambda^{\frac{5}{4}}\beta^{\frac{3}{4}} \mid \varepsilon^3 C_{\mathrm{REF}}^{\frac{3}{8}} (T_{\mathrm{REF}}/T_\infty)^{\frac{3}{2}} (T_w/T_{\mathrm{REF}})^{\omega+\frac{1}{2}} \quad (1)$$

$$\hat{Y} \equiv (Y/L)\lambda^{\frac{3}{4}}\beta^{\frac{1}{4}} \mid \varepsilon^5 C_{\mathrm{REF}}^{\frac{5}{8}} (T_{\mathrm{REF}}/T_\infty)^{\frac{3}{2}} (T_w/T_{\mathrm{REF}})^{\omega+\frac{1}{2}} \quad (2)$$

$$\hat{U} \equiv (U/U_\infty)\beta^{\frac{1}{4}} \mid \varepsilon C_{\mathrm{REF}}^{\frac{1}{8}} \lambda^{\frac{1}{4}} (T_w/T_\infty)^{\omega+\frac{1}{2}} \quad (3)$$

$$\hat{V} \equiv (V/U_\infty)\,|\,\varepsilon^3\beta^{\frac{1}{4}}C_{\mathrm{REF}}^{\frac{3}{8}}\lambda^{\frac{3}{4}}(T_w/T_\infty)^{\frac{1}{2}} \tag{4}$$

$$\hat{p} \equiv \left[(p-p_\infty)\,|\,\rho_\infty U_\infty^2\right]\beta^{\frac{1}{2}}\,|\,\varepsilon^2 C_{\mathrm{REF}}^{\frac{1}{4}}\lambda^{\frac{1}{2}} \tag{5}$$

$$\hat{H} \equiv \beta^{\frac{1}{4}}(H - C_pT_w)\,|\,Pr^{\frac{1}{3}}(H_{\mathrm{AD}} - C_pT_w)\varepsilon C_{\mathrm{REF}}^{\frac{1}{8}}\lambda^{\frac{1}{4}}(T_w/T_\infty)^{\frac{1}{2}} \tag{6}$$

where T_{REF} is evaluated according to Eckert for air ($Pr = 0.72$) as

$$T_{\mathrm{REF}}/T_\infty \cong 0.50 + 0.039M_\infty^2 + 0.50(T_w/T_\infty) \tag{7}$$

On neglecting certain terms associated with very large degrees of cooling that can be shown[5] to be insignificant under most conditions of practical interest, the resulting rescaled flow equations describing the dynamic and thermal interactive disturbances are as follows in the leading asymptotic approximation as $\varepsilon \to 0$:

$$\frac{\partial \hat{U}}{\partial \hat{X}} + \frac{\partial \hat{V}}{\partial \hat{Y}} = 0 \tag{8}$$

$$\hat{U}\frac{\partial \hat{U}}{\partial \hat{X}} + \hat{V}\frac{\partial \hat{U}}{\partial \hat{Y}} + \frac{\mathrm{d}\hat{p}}{\mathrm{d}\hat{X}}\frac{H}{H_w} = \frac{\partial^2 \hat{U}}{\partial \hat{Y}^2} \tag{9}$$

$$\hat{U}\frac{\partial \hat{H}}{\partial \hat{X}} + \hat{V}\frac{\partial \hat{H}}{\partial \hat{Y}} = P_r^{-1}\frac{\partial^2 \hat{H}}{\partial \hat{Y}^2} \tag{10}$$

where a term proportional to $(U_0/U_\infty)^2$ has been neglected compared to unity in the coefficient of $\mathrm{d}p/\mathrm{d}X$ in Eq. (9), whereas in Eq. (10) a term proportional to $(1 - P_r)\partial/\partial y(u\partial u/\partial y)$ has also been neglected (a well-known accurate approximation even in very strongly bhypersonic flow[6]). The impermeable wall boundary conditions on the solution to these equations are those of no slip $\hat{U}(\hat{X}, 0) = \hat{V}(\hat{X}, 0) = 0$ plus the imposed thermal jump across X_J that $\hat{H}(\hat{X} < \hat{X}_J, 0) = \hat{H}_w^-$, $\hat{H}(\hat{X} \geq \hat{X}_J, 0) = \hat{H}_w^-[1 + (\Delta T_w/T_w^-)]$. The corresponding heat transfer is determined from the resulting value of $\partial\hat{H}/\partial\hat{Y}$ at the wall and the reverse of transformations Eqs. (2) and (6) applied to the basic relation

$$-\dot{q}_w = \frac{\mu_w}{P_r}\frac{\partial H}{\partial y}(x, 0) \tag{11}$$

The third step in the formulation is to provide outer boundary conditions in the form of appropriate matching conditions with the inner behavior as ($y \to 0$) of the overlying middle deck. On using the rotational inviscid flow equations pertaining to the middle deck as $\varepsilon \to 0$, combined with a tangent wedge model of the pressure-deflection angle relationship for the local external inviscid flow, these matching conditions are found to be

$$\hat{V}(\hat{X}, \hat{Y} \to \infty) = \hat{s}_e\hat{y} \tag{12}$$

$$\hat{U}(\hat{X}, \hat{Y} \to \infty) = \hat{H}(\hat{X}, \hat{Y} \to \infty) = \hat{y} - \int_{-\infty}^{\hat{X}} \hat{s}_e\,\mathrm{d}\hat{X} \tag{13}$$

where

$$\hat{y} \cong \hat{Y} + \int_0^{\hat{Y}\to\infty}\left(\left(\frac{\hat{H}}{\hat{H}_w^-}\right) - 1\right)\mathrm{d}\hat{Y} \tag{14}$$

contains the displacement effect of the wall temperature jump. [Equations (12) and (14) are of key importance in understanding the interactive physics generated by a wall temperature jump; they show that the cumulative inner deck compressibility effect due to a T_w increase causes a vertical velocity disturbance and, hence, an upward displacement of the overlaying decks.] The disturbance flow slope is linked to the pressure by

$$\hat{p} = \hat{s}_e\left[\sqrt{1 + (K_H\hat{s}_e)^2} + K_H\hat{s}_e\right] \tag{15}$$

involving the local viscous interaction parameter K_H that is proportional to the global interaction parameter $\bar{\chi}^{1/2}$. Note that Eq. (15) generalizes the $\hat{p}$ vs $\hat{s}_e$ relationship of classical triple-deck theory to the case of arbitrary hypersonic Mach numbers; in the limit $K_H \to 0$ it passes over to the usual linearized supersonic result $\hat{p} = \hat{s}_e$.

The fourth step in the setup is the realization that the discontinuous nature of the thermal boundary condition requires a splitting of the enthalpy solution into two parts, one accommodating directly the wall temperature jump and the other containing the upstream influence effect plus an ability to provide matching with the middle deck. Some preliminary study indicates that such a decomposition takes the specific form

$$\hat{H} = \hat{H}_w^-\left[1 + J\left(\Delta T_w/T_w^-\right)\cdot\theta(\hat{X}, \hat{Y})\right] + \varepsilon\hat{H}(X, Y) \tag{16}$$

with $J = 0$ or 1 for $\hat{X} < 0$ or $\hat{X} > 0$, respectively, and where we require $\theta(x, 0) = 1$, $\hat{H}(X, 0) = 0$, and $\theta(X, Y \to \infty) = 0$.

B. Linearization of the Problem

The final step is to restrict attention to the case of small fractional temperature jumps, thereby linearizing the problem. This situation is often the case in practice and in any event is formally justified by $\Delta T_w/T_w^-$ having to be $0(\varepsilon)$ in smallness [Eq. (16)] to the leading order of asymptotic approximation used. Consistent with this, we also adopt the weak interaction limit $K_H \to 0$ of Eq. (15) pertaining to linearized supersonic inviscid flow in the outer deck.

Such linearization is conveniently implemented by introducing a new set of dependent perturbation variables $\mathcal{U}$, $\mathcal{V}$, $\mathcal{P}$, and $\mathcal{H}$, defined by taking

$$\hat{U} = (\hat{Y}) + \left(\Delta T_w\,|\,T_w^-\right)\cdot\mathcal{U}(\hat{X}, \hat{Y}) \tag{17}$$

$$\hat{V} = \left(\Delta T_w\,|\,T_w^-\right)\cdot\mathcal{V}(\hat{X}, \hat{Y}) \tag{18}$$

$$\hat{H} = \left(1 - J\left(\frac{H_w^-}{H_{\mathrm{AD}} - H_w^-}\right)\frac{\Delta T_w}{T_w^-}\right)\hat{Y} + \frac{\Delta T_w}{T_w^-}\mathcal{H}(\hat{X}, \hat{Y}) \tag{19}$$

$$\hat{p} = \left(\Delta T_w\,|\,T_w^-\right)\cdot\mathcal{P}(\hat{x}) \tag{20}$$

Then, substituting these into the preceding formulation and then neglecting second- and higher-order terms in $\Delta T_w/T_w^-$, we obtain a set of universal split boundary value problems that govern the nondimensional θ, $\mathcal{U}$, $\mathcal{V}$, $\mathcal{H}$, and $\mathcal{P}$ perturbation distribution functions. The θ field associated with the direct effect of the wall temperature jump (which introduces no upstream influence) is independent of the rest and is governed by the classical Airy-type of differential equation

$$\hat{Y}\frac{\partial\theta}{\partial\hat{X}} = Pr^{-1}\left(\frac{\partial^2\theta}{\partial\hat{Y}^2}\right) \tag{21}$$

subject to the downstream boundary conditions that $\theta(X, 0) = J$ and $\theta(X, \hat{Y} \to \infty) = 0$. The small velocity and pressure perturbation fields, which introduce upstream influence, are governed by the pair of well-known linearized triple-deck equations

$$\frac{\partial\mathcal{U}}{\partial\hat{X}} + \frac{\partial\mathcal{V}}{\partial\hat{Y}} = 0 \tag{22}$$

$$\hat{Y}\frac{\partial\mathcal{U}}{\partial\hat{X}} + \mathcal{V} + \frac{\mathrm{d}\mathcal{P}}{\mathrm{d}\hat{X}} = \frac{\partial^2\mathcal{U}}{\partial\hat{Y}^2} \tag{23}$$

subject to the no-slip impermeable wall boundary conditions $\mathcal{U}(\hat{X}, 0) = \mathcal{V}(\hat{X}, 0) = 0$ and the nonhomogeneous outer matching condition

$$\mathcal{U}(\hat{X}, \hat{Y} \to \infty) = \int_0^\infty \theta\,\mathrm{d}\hat{Y} - \int_{-\infty}^{\hat{X}} \mathcal{P}\,\mathrm{d}\hat{X}$$

involving the total integrated θ field across the inner deck as the driving effect. Finally, the attendant enthalpy perturbation field that also exhibits upstream influence (being driven by the pressure disturbance) is governed by

$$\hat{Y}\frac{\partial \mathcal{H}}{\partial \hat{X}} + \mathcal{V} = (Pr^{-1})\frac{\partial^2 \mathcal{H}}{\partial \hat{Y}^2} \tag{24}$$

subject to the conditions

$$\mathcal{H}(\hat{X}, 0) = 0, \qquad \mathcal{H}(\hat{X}, \hat{Y} \to \infty) = -\int_{-\infty}^{\hat{X}} \mathcal{P}\, \mathrm{d}\hat{X}$$

C. Closed-Form Solution by Fourier Transformation

The foregoing linear boundary value problems are of a type that has frequently arisen in triple-deck theory. In particular, they have proven amenable to elegant analytical solution by the Fourier transform method (see, for example, Refs. 7–9). The same approach was, therefore, applied here as well.

Referring the interested reader to the references for the typical details, taking the Fourier transformation with respect to $\hat{X}$ produces a set of Airy-type ordinary differential equations that possesses closed-form solutions. Subsequent application of the inversion process in concert with the residue theorem and careful attention to contour integration for the downstream aspect of the problem then ultimately leads to closed-form expressions for the unknown surface property distributions. In the present work, application of this procedure specifically to Eqs. (21–24) produces the following final results for the scaled wall pressure and heat transfer distributions. In the region $X < X_J (\hat{X} < 0)$ upstream of the temperature jump, the behavior is exponential in nature:

$$\hat{p}(\hat{X}) = C_1\left(\Delta T_w \mid T_w^-\right) e^{\kappa \hat{X}} \tag{25}$$

$$\hat{q} = \dot{q}_w / \dot{q}_{w_0} = 1 - C_2\left(\Delta T_w \mid T_w^-\right) e^{\kappa \hat{X}} \tag{26}$$

where $\kappa = 0.827$ is a universal constant and the constants C_1 and C_2 are given in the Appendix. Downstream of the jump ($\hat{X} > 0$) the behavior is more complicated, culminating in fractional power law decay in the far wake, as follows:

$$\hat{p}(\hat{X}) = C_3\left(\frac{\Delta T_w}{T_w^-}\right)\int_0^\infty \frac{\left(t + t^{-\frac{1}{3}}\right)e^{-\kappa t \hat{X}}}{t^{\frac{8}{3}} + t^{\frac{4}{3}} + 1}\, \mathrm{d}t \tag{27a}$$

$$\simeq C_4\left(\Delta T_w \mid T_w^-\right)(\hat{X})^{-\frac{2}{3}} \tag{27b}$$

for large $\hat{X}$ and

$$\hat{q} = 1 - \left(\frac{\Delta T_w}{T_w^-}\right)\left\{\left(\frac{H_w^-}{H_{\mathrm{AD}} - H_w^-}\right)\left(1 + \frac{C_5}{\varepsilon(\hat{X})^{\frac{1}{3}}}\right) - C_6\int_0^\infty \frac{t^{\frac{1}{3}} e^{-\kappa t \hat{X}}\, \mathrm{d}t}{t^{\frac{8}{3}} + t^{\frac{4}{3}} + 1}\right\} \tag{28}$$

where the constants $C_2, \ldots, C_6$ are also given in the Appendix. Note that when $\hat{X} \gg 1$ the integral coefficient of C_6 in Eq. (28) takes the negligibly small value $\Gamma(\frac{4}{3})(\kappa\hat{X})^{-4/3}$. These analytical results will be directly compared with the purely CFD predictions and discussed in detail hereafter.

IV. Navier–Stokes Numerical Simulation

A. Code Description

The CFD solutions are provided by LAURA.[2] Validating comparisons of this code with experimental data for hypersonic flows in air are well documented in the literature.[10–17] The code employs upwind-biased, point-implicit relaxation. Inviscid fluxes are approximated with Roe's averaging,[15] eigenvalue limiting similar to that of Harten,[16] and Yee's symmetric total variation diminishing scheme.[17] Viscous fluxes are approximated with central differences.

Although a space marching code would normally be sufficient for describing flow on a flat plate, it is not appropriate for the present study because identification of upstream influences of the surface temperature jump is of primary concern. Consequently, global relaxation of the governing equations is employed.

B. Grid Convergence

Sequences of successively finer streamwise girds were used to resolve the flow in the immediate neighborhood of the temperature jump. The initial grid used 200 cells from the leading to trailing edge of the plate, and subsequent grids picked up converged solutions of the flow sufficiently upstream of x_J to preclude any upstream effects of the jump on the flow profiles. The simulations used 128 cells across the shock layer; comparisons to a 64-cell simulation indicate grid convergence. The outer boundary is aligned with the shock emanating from the leading edge. The cell Reynolds number at the wall averaged 0.25. The maximum stretching factor in the normal direction was 1.12 occurring near the middle of the boundary layer at $k = 50$.

As noted, the initial coarsest grid uses (200 × 128) cells, providing streamwise resolution near x_J of approximately 3 mm. The next grid in sequence uses a single cell deep feeder block and a single, refined block (200 × 128) extracted from the coarser block to resolve upstream and downstream influence of the temperature jump at X_J. This provides streamwise resolution around x_J of approximately 0.3 mm.

The finest grid uses a single cell deep feeder block and three active blocks (89 × 128), (128 × 128), and (90 × 128), resolving the shock layer near X_J. The second of these active blocks provides another factor-10 increase in streamwise resolution near X_J to approximately 0.03 mm. This grid and associated simulation of pressure contours in the constant wall temperature case is shown in Fig. 3.

C. Application to a Wall Temperature Jump

The imposition of an abrupt 10% increase in wall temperature at x_J induces changes in pressure and heating that are felt upstream as well as in the wake of the discontinuity. As illustrated in Fig. 4, the pressure jump is largest at X_J and the perturbation moves up to the boundary-layer edge. A tiny (0.003 times the wall jump-induced perturbation) pressure oscillation that had been observed in the constant wall temperature calculation now disappears, being overwhelmed by the much larger gradients in interactive pressure. A broader perspective of this interaction field can be seen in Fig. 2, which was presented in the Introduction.

The numerically simulated pressure and heating distributions along the surface are replotted in unscaled form vs the transformed coordinate $\hat{X}$ in Fig. 6 for both a constant wall temperature and with the wall temperature jump. The highly resolved regions both upstream and downstream of X_J are evident in Fig. 6, as are the pronounced local pressure rise and corresponding sharp heating spike generated by the temperature discontinuity. Another interesting feature to be seen in Fig. 6 is the occurrence of a very small residual pressure shift in the asymptotic region far downstream, caused by the very weak background inviscid pressure gradient that persists downstream of the blunt nose of the plate being carried across the interaction zone as indicated in Fig. 6.

V. Results and Discussion

A. Comparison of Analytical and CFD Solutions

A direct comparison of the present triple-deck theory with the foregoing Navier–Stokes numerical solution for the nondimensional scaled pressure distribution $\hat{p}(\hat{x})$ is shown in Fig. 7 for the Mach 2 case. It is seen that the shape, extent, and magnitude of the pressure perturbation are all very accurately predicted by the triple-deck theory throughout both the upstream influence and downstream wake regions of the interaction. The same excellent comparisons are also obtained for the corresponding nondimensional heat transfer predictions, as shown in Fig. 8; in particular, the theory is clearly able to capture properly the important sharp peaking of the local heating that occurs immediately downstream of the temperature jump, as well as the slow subsequent approach in the wake toward the proper asymptotic value pertaining to the higher jumped wall temperature. The sharp peak in heating is caused by the $(\hat{X})^{-1/3}$ singular behavior associated with the θ component of the energy equation solution [Eqs. (16), (21), and (28)]; it presumably would be mitigated by the even smaller-scale effects of streamwise diffusion.

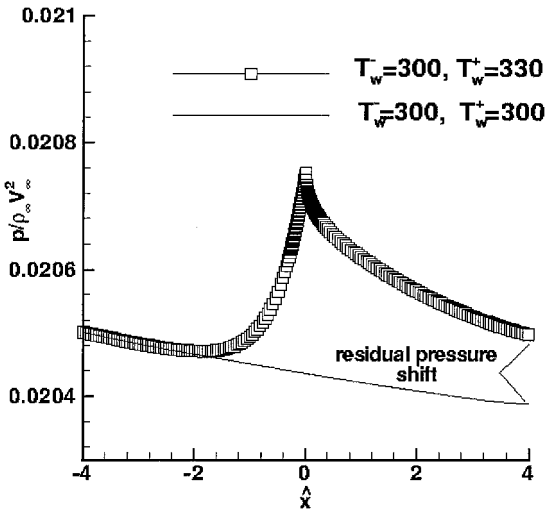

Pressure

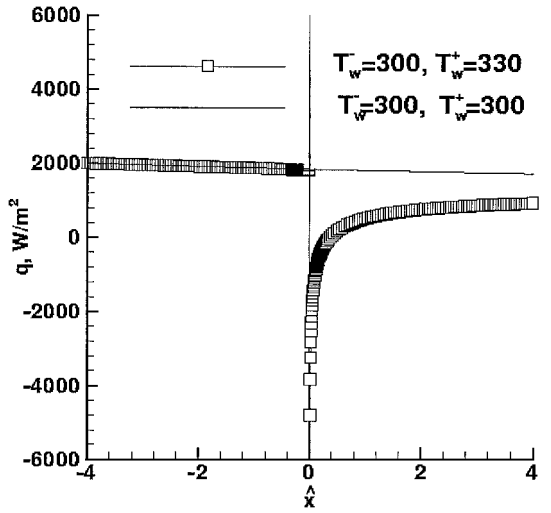

Heating

Fig. 6 Typical interactive pressure and heating distributions for a weak T_w increase compared to the noninteractive CFD solutions.

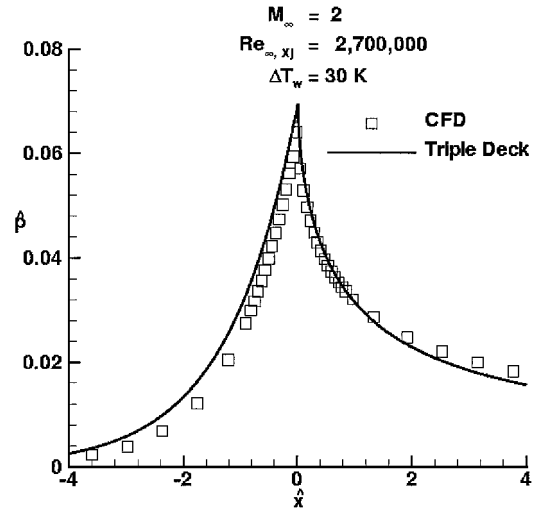

Fig. 7 Comparison of pressure distribution along wall with temperature jump as predicted by triple-deck theory and numerical simulation.

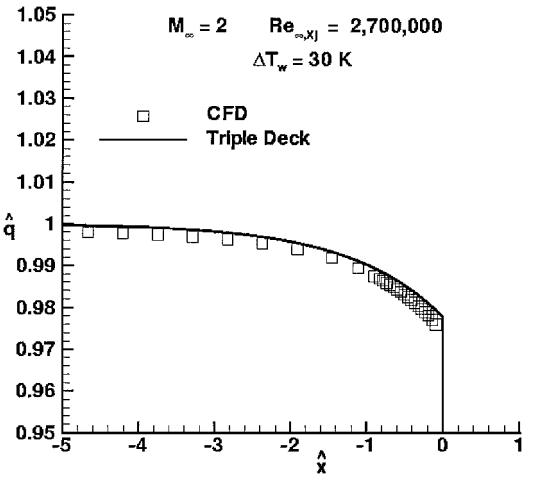

Upstream of jump

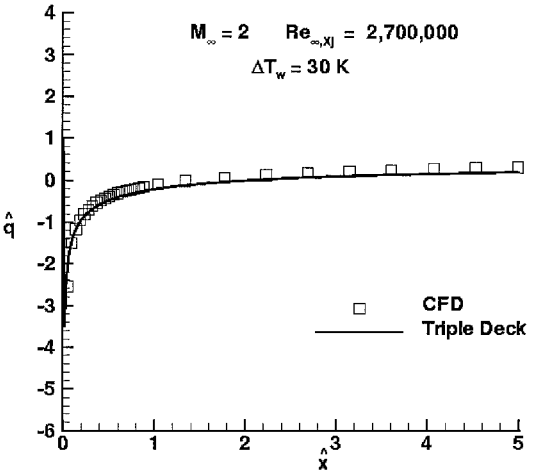

Downstream of jump

Fig. 8 Comparison of heating distribution along wall with temperature jump as predicted by triple-deck theory and numerical simulation.

B. Anatomy of the Interaction

The foregoing validation of the accuracy of the triple-deck theory solution now affords the opportunity to exploit its closed form to further illuminate the physics of the downstream interaction field. This has been done in Fig. 9, where the theory is broken down into its component contributions according to Eqs. (27) and (28). This clearly brings out how the short-ranged interactive pressure gradient and the associated rapid peaking of the local heating becomes negligible beyond $\hat{X} \simeq 3$, leaving a slowly decaying constant pressure heat transfer wake that is the downstream tail of the jump-effect component of the triple-deck solution. Note that even the already small streamwise scale of both the triple-deck theory and the present Navier–Stokes calculations still contains a discontinuous pressure gradient and heat transfer immediately across the jump; presumably smoothing these out would entail proceeding to an even smaller ΔX scale astride the jump and incorporating streamwise viscous $(\partial^2 U/\partial X^2)$ and heat conduction $(\partial^2 T/\partial X^2)$ terms.

This closer examination also affords the opportunity to compare the triple-deck theory against a well-known integral method treatment of the temperature jump problem based on classical boundary-layer theory.[18] Under the assumption of zero streamwise pressure gradients and zero upstream influence, the latter yields the following approximate analytical expression for the heat transfer variation downstream of the jump:

$$\hat{q} \cong 1 - \left[H_w^-\right| \left(H_{\mathrm{AD}} - H_w^-\right)\left](\Delta T_w\right| T_w^-\left)\left[1 - (X_J/X)^{\frac{3}{4}}\right]^{-\frac{1}{3}} \quad (29)$$

Far downstream, where $X \gg X_J$, this expression approaches the correct asymptotic value pertaining to the postjump wall temperature, in agreement with the triple-deck result (28). Furthermore, given

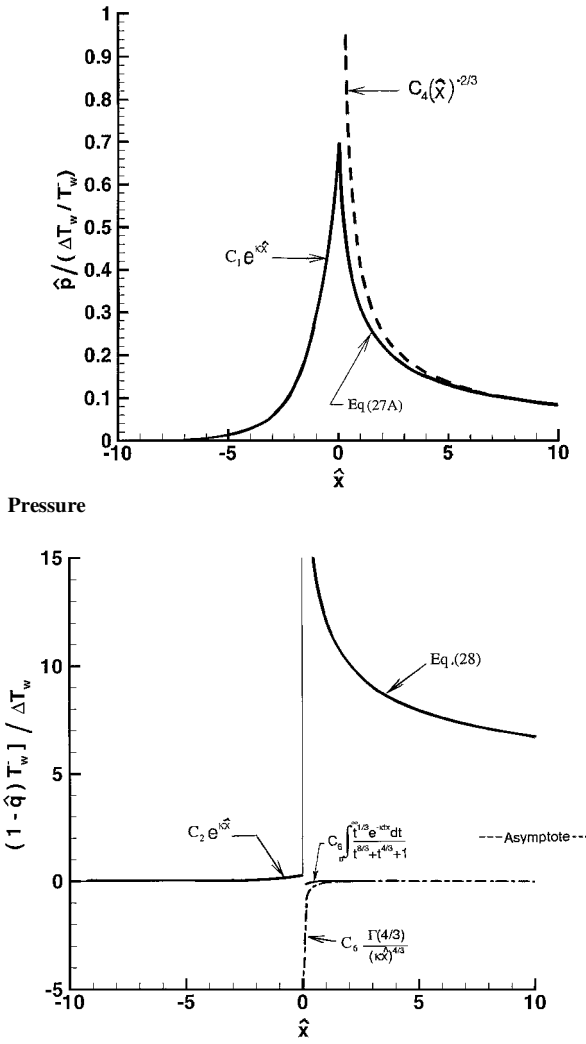

Fig. 9 Anatomy of the interaction solution with breakdown of analytic contributions.

its underlying isobaric nature, we might expect that Eq. (29) would also describe the constant pressure far wake behavior of the interactive solution. To check this, we rewrite the outer expression (29) in terms of the inner triple-deck variable $\hat{X}$; setting $X_J = L$ we get in the limit $\varepsilon \to 0$ that

$$\hat{q} \simeq 1 - \left[H_w^-|\ \left(H_{\mathrm{AD}} - H_w^-\right)\right] \times \left\{\left[C_7 \beta^{\frac{1}{4}}|\ \lambda^{\frac{1}{4}} C_{\mathrm{REF}}^{\frac{1}{8}} (T_w/T_{\mathrm{REF}})^{\frac{1}{2}} \varepsilon [\hat{X}]^{\frac{1}{3}}\right] + 1\right\}\left(\Delta T_w|\ T_w^-\right) \tag{30}$$

where $C_7 = (\frac{4}{3})^{1/3}\lambda^{2/3} = 0.528$. This is now compared with the triple-deck result of Eq. (28) pertaining to the downstream constant pressure wake region of the interaction, which can be written in the comparable form

$$\hat{q} \simeq 1 - \left[H_w^-|\ \left(H_{\mathrm{AD}} - H_w^-\right)\right] \times \left\{\left[C_8 \beta^{\frac{1}{4}}|\ \lambda^{\frac{1}{4}} C_{\mathrm{REF}}^{\frac{1}{8}} (T_w/T_{\mathrm{REF}})^{\frac{1}{2}} \varepsilon [\hat{X}]^{\frac{1}{3}}\right] + 1\right\}\left(\Delta T_w|\ T_w^-\right) \tag{31}$$

with $C_8 \equiv 0.729\sqrt{(3)}\Gamma\frac{1}{3}/2\pi = 0.538$ and where the $(\hat{X})^{-1/3}$ term dominates as $\hat{X} \to 0$. Note that Eqs. (30) and (31) in the leading $\varepsilon \to 0$ approximation predict exactly the same basic dependence on all of the basic parameters of the problem including the $(\hat{X})^{-1/3}$ decay with downstream distance, differing only slightly in a numerical constant. That there should be some difference between them is understandable in view of the drastically different upstream flow histories involved. Whereas the boundary-layer result (30) involves

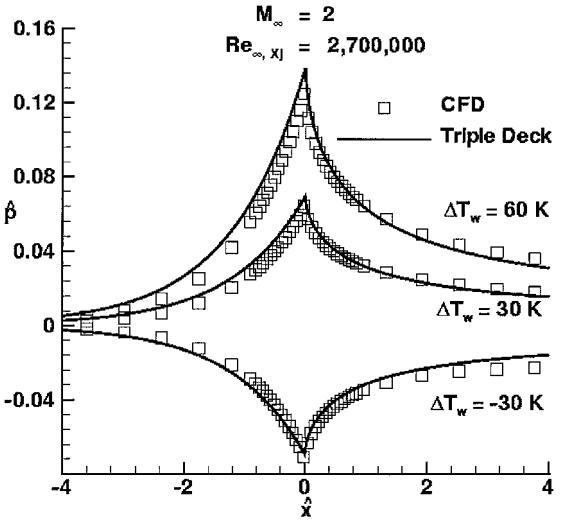

Fig. 10 Effect of temperature jump amplitude on interactive pressure distribution.

no pressure gradient whatsoever, the triple-deck solution (31) results from a strongly interactive upstream history including upstream influence.

C. Influence of Temperature Amplitude

Physical intuition and the preceding triple-deck solutions would both suggest that the strength of the interaction is directly proportional to the sign and magnitude of the nondimensional temperature jump $\Delta T_w / T_w^-$, and this is indeed confirmed by the Navier–Stokes solution results for three different ΔT_w as shown in Figs. 10 (pressure) and 11 (heating). In all cases, the triple-deck theory gives a satisfactory account of both the local pressure and heat transfer perturbation field including the situation where a wall temperature decrease produces an expansive (rather than compressive) disturbance. Also note that the earlier mentioned slight downstream post-interaction pressure shift associated with the small background inviscid pressure gradient grows in proportion to the strength of the interaction, that is, to ΔT_w, as one would expect.

D. Further Parametric Studies: Effects of Reynolds and Mach Numbers

The application of the leading asymptotic approximation ($\varepsilon \to 0$) of triple-deck theory at finite Reynolds numbers introduces some error that may be assessed by comparing with the numerical solutions of the Navier–Stokes and thin-layer Navier–Stokes equations. This is done in Fig. 12, where the Mach 2, 10% temperature jump pressure distributions $\hat{p}(\hat{x})$ at two different practical Reynolds numbers are compared with the triple-deck result for $Re_L \to \infty$. It can be seen that the finite Reynolds number effect serves to reduce slightly the streamwise extent of the interaction in $\hat{x}$, primarily in the upstream influence region, the reduction increasing with decreasing Reynolds number Re_L. This effect stems from the fact that, in contrast to what is assumed in the triple-deck model, the upstream region of any real interaction depends on conditions at the upstream start of the interaction rather than at $X = L$; as discussed by Stewartson,[3] this leads to a modest Reynolds number effect that reduces the effective upstream influence distance in $\hat{x}$. The present results for the temperature jump problem are also in qualitative agreement with an earlier theoretical study[19] of finite Reynolds number effects on oblique shock-generated interactions.

Turning to a consideration of the Mach number effect, Fig. 13 presents a comparison of the 10% temperature jump triple-deck scaled pressure distribution with the CFD solutions obtained at three different $M_\infty = 2$, 4, and 6. [The nondimensional triple-deck Eqs. (8–10) are independent of M_∞ in the present leading order of asymptotic approximation.] Note that as the freestream Mach number increases and enters the hypersonic regime, the numerical solution of the full equation set predicts a progressively more significant reduction in upstream influence along with a modest reduction

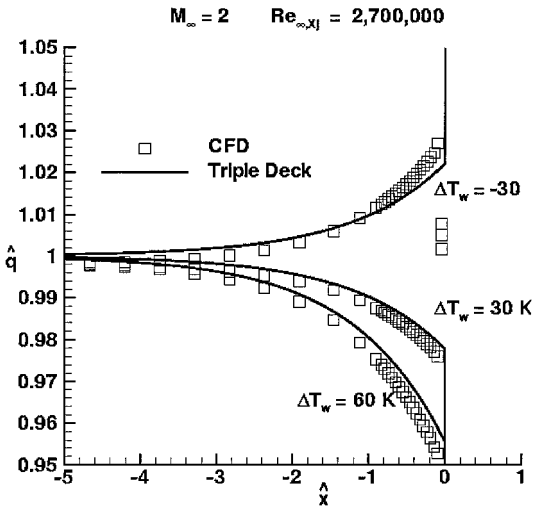

Upstream of jump

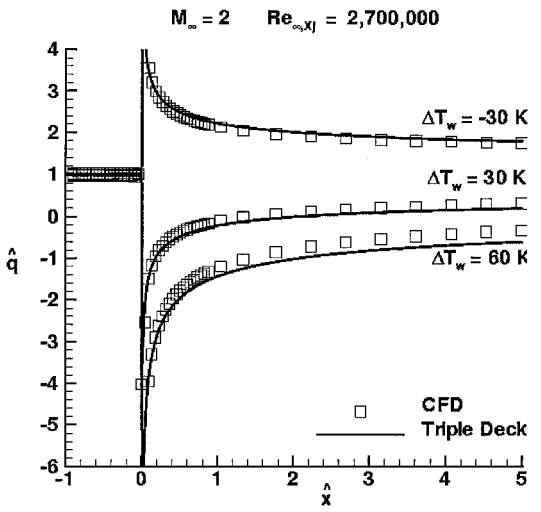

Downstream of jump

Fig. 11 Effect of temperature jump amplitude on interactive heating distribution.

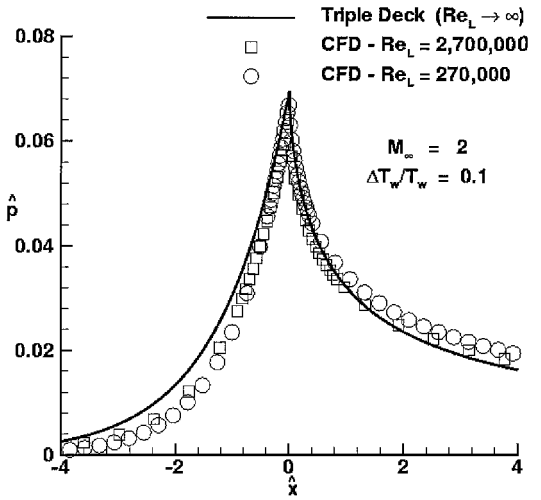

Fig. 12 Finite Reynolds number effect on the interactive pressure field.

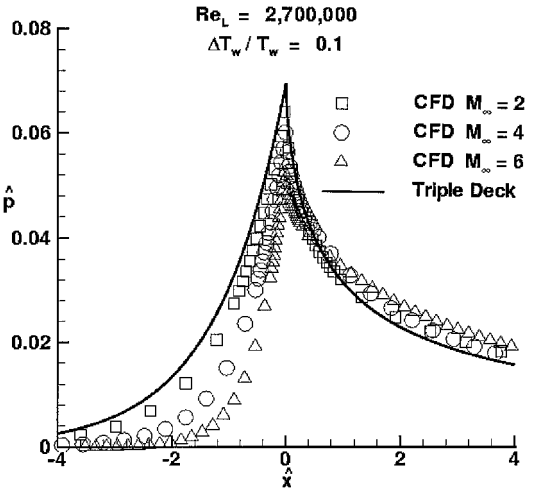

Pressure

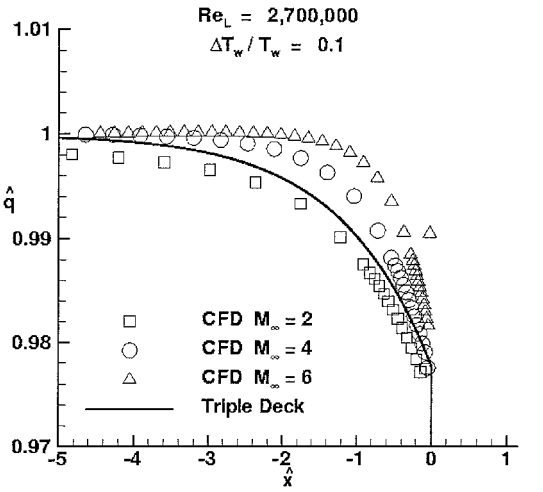

Upstream heat transfer

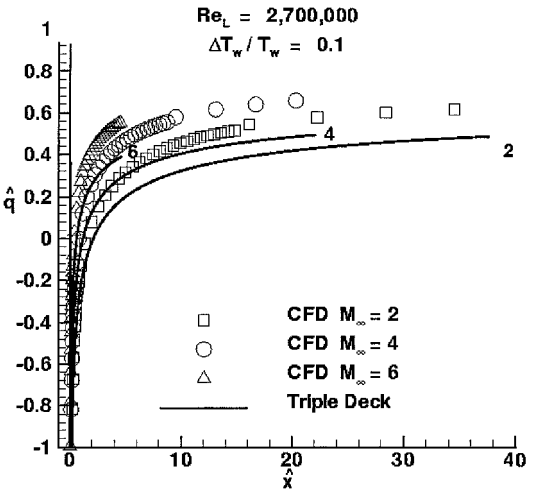

Downstream heat transfer

Fig. 13 Mach number effect on triple-deck theory and CFD simulation.

in the corresponding maximum pressure. Analysis indicates that this Mach number effect is the combined result of nonlinear effects in both the inviscid pressure-flow deflection relationship and the temperature jump interaction (neither of which are accounted for in the present linearized treatment) plus the Mach number sensitivity of the aforementioned dependence of the interaction on conditions at the start of upstream influence instead of at $X = L$. Interestingly, there is little attendant Mach number effect on the downstream wake behavior. Also note that the local heat transfer behaves similarly to the pressure as regards these Mach number effects.

VI. Conclusions

This paper has presented a new analytical theory of wall temperature jump-generated interactions in supersonic flow that captures all of the major physics of the resulting pressure and local heat transfer behavior, including upstream influence. Validating comparisons with Navier–Stokes numerical solutions were given that

establish confidence that the closed-form analytical results may be used effectively as a locally interuptive module within a larger-scale CFD design code to avoid costly resolution of the small-scale interaction physics (especially heat transfer) by the code.

An obviously related problem to the present one is that of dissociated gas flow past a wall with a jump in the surface catalycity (heterogeneous recombination rate). This situation arises in connection with thermal protection system design for hypervelocity vehicles operating in the high-altitude nonequilibrium flow chemistry regime where there is a discontinuity in the surface material at some station along the body. A preliminary treatment of this problem based on classical boundary-layer theory (neglecting any pressure interaction or upstream influence) has been presented already by the present authors[1]; the present work now points the way to extend this analysis to include the interactive aspects. A complete analytical treatment of the catalytic jump problem using a triple-deck approach is currently nearing completion (although similar in many respects, certain of its details are more complicated than the temperature jump problem). This work, like the present, will include direct comparisons with Navier–Stokes numerical solutions across the jump.

Appendix: Constants in the Triple-Deck Analytical Solutions

In Eqs. (25–28), we have

$$C_1 = \tfrac{3}{4} \times 0.729 \mid Pr^{\frac{1}{3}} \kappa^{\frac{2}{3}}$$

$$C_2 = \tfrac{3}{4} \times 0.315[1 + 0.196(1 - Pr)]$$

$$C_3 = \sqrt{3} \times 0.729 \mid 2\pi Pr^{\frac{1}{3}} \kappa^{\frac{2}{3}}$$

$$C_4 = \sqrt{3} \times 0.729\Gamma(2/3) \mid 2\pi Pr^{\frac{1}{3}} \kappa^{\frac{4}{3}}$$

$$C_5 = \sqrt{3} \times 0.729\Gamma(1/3)\beta^{\frac{1}{4}} \mid 2\pi \lambda^{\frac{1}{4}} C_R^{\frac{1}{8}} (T_w / T_\infty)^{\frac{1}{2}}$$

$$C_6 = \tfrac{4}{3}\sqrt{3} C_2 \mid 2\pi$$

Acknowledgment

The partial support for the first author's work by NASA Grant NAG-11807 is gratefully acknowledged.

References

[1]Inger, G. R., and Gnoffo, P. A., "Hypersonic Entry Heating with Discontinuous Surface Catalycity: A Combined Analytic/CFD Approach," AIAA Paper 96-2150, June 1996.

[2]Gnoffo, P. A., "An Upwind-Biased, Point-Implicit Relaxation Algorithm for Viscous Compressible Perfect Gas Flows," NASA TP 2953, Feb. 1990.

[3]Stewartson, K., "Multistructured Boundary Layers on Flat Plates and Related Bodies," *Advances in Applied Mechanics*, Vol. 14, 1971, pp. 145–239.

[4]White, F., *Viscous Fluid Flow*, 2nd ed., McGraw–Hill, New York, 1991, pp. 511–513.

[5]Inger, G. R., "Theory of Local Heat Transfer in Shock/Laminar Boundary-Layer Interactions," *Journal of Thermophysics and Heat Transfer*, Vol. 12, No. 3, 1998, pp. 336–342.

[6]Hayes, W. D., and Probstein, R. F., *Hypersonic Flow Theory*, Academic Press, New York, 1959, p. 277.

[7]Smith, F. T., "Laminar Flow over a Small Hump on a Flat Plate," *Journal of Fluid Mechanics*, Vol. 57, 1973, pp. 803–824.

[8]Smith, F. T., and Stewartson, K., "On Slot Injection into a Supersonic Laminar Boundary Layer," *Proceedings of the Royal Society of London, Series A: Mathematical and Physical Sciences*, Vol. 332, 1973, pp. 1–22.

[9]Rizzetta, D. P., "Asymptotic Solutions of the Energy Equation for Viscous Supersonic Flow Past Corners," *Physics of Fluids*, Vol. 22, No. 1, 1979, pp. 218–223.

[10]Gnoffo, P. A., "Code Calibration Program in Support of the Aeroassist Flight Experiment," *Journal of Spacecraft and Rockets*, Vol. 27, No. 2, 1990, pp. 131–142.

[11]Weilmuenster, K. J., and Gnoffo, P. A., "Aeroassisted Flight Experiment Aerodynamic Characteristics at Flight Conditions," *Journal of Spacecraft and Rockets*, Vol. 27, No. 6, 1990, pp. 684–686.

[12]Thompson, R. A., and Gnoffo, P. A., "Application of the LAURA Code for Slender Vehicle Aerothermodynamics," *Journal of Spacecraft and Rockets*, Vol. 29, No. 1, 1992, pp. 16–23.

[13]Weilmuenster, K. J., Gnoffo, P. A., and Greene, F. A., "Navier–Stokes Simulations of Orbiter Aerodynamics Characteristics Including Pitch Trim and Bodyflap," *Journal of Spacecraft and Rockets*, Vol. 31, No. 3, 1994, pp. 355–366.

[14]Gnoffo, P. A., Weilmuenster, K. J., and Alter, S. J., "Multiblock Analysis for Shuttle Orbiter Reentry Heating from Mach 24 to Mach 12," *Journal of Spacecraft and Rockets*, Vol. 31, No. 3, 1994, pp. 367–377.

[15]Roe, P. L., "Approximate Reimann Solvers, Parameter Vectors, and Difference Schemes," *Journal of Computational Physics*, Vol. 43, No. 10, 1981, pp. 357–372.

[16]Harten, A., "High Resolution Schemes for Hyperbolic Conservation Laws," *Journal of Computational Physics*, Vol. 49, No. 2, 1983, pp. 357–393.

[17]Yee, H. C., "On Symmetric and Upwind TVD Schemes," NASA TM 88325, June 1986.

[18]Bejan, A., *Convection Heat Transfer*, Wiley, New York, 1984, pp. 53–57.

[19]Hussaini, M. Y., Baldwin, B. S., and McCormack, R. L. V., "Asymptotic Features of Shock Wave–Boundary Layer Interaction," *AIAA Journal*, Vol. 18, No. 18, 1980, pp. 1014–1016.

M. Sichel
Associate Editor